Journal of Electron Spectroscopy and Related Phenomena xxx (xxxx) xxx–xxx

Contents lists available at ScienceDirect

Journal of Electron Spectroscopy and Related Phenomena

journal homepage: www.elsevier.com/locate/elspec

SEY and low-energy SEY of conductive surfaces

R. Cimino[a,*], M. Angelucci[a], L.A. Gonzalez[a], R. Larciprete[b,a]

[a] LNF-INFN, P.O. Box 13, 00044 Frascati, Roma, Italy
[b] CNR-ISC Istituto dei Sistemi Complessi, Via dei Taurini 19, 00185 Roma, Italy

A B S T R A C T

The study of Secondary Electron Yield (SEY) is widely performed to address important properties of materials to be used in a very wide spectrum of applications. It is, therefore, extremely important to understand the SEY dependence on material type, surface contaminants, structural quality and surface damage. We review here our recent studies of such items performed by looking at some representative conductive materials as noble metals and carbon based surfaces. Polycrystalline Ag, Au and Cu samples have been studied as introduced in the ultra-high vacuum chamber (therefore with an significant surface contamination) and after having been cleaned by ion sputtering. The comparison between the curves confirms that the SEY behavior is strongly influenced by the chemical state of the metal surfaces. We demonstrate the ability of SEY to determine work function values with high accuracy if the experimental system allows using very slow primary electrons. We also investigated, for the Cu sample, the effect on SEY of minimal amount of contaminants in the sub-monolayer regime showing that SEY is highly sensitive to the presence of adsorbates even at such very low coverages, specially for low energy primary electrons. In the case of C surfaces we summarize here the effect that the structural ordering of the C lattice has on the macroscopic SEY properties of ultrathin C layers. In particular we followed the SEY evolution during the thermal graphitization of thin amorphous carbon layers and during the amorphization of highly oriented pyrolytic graphite by means of Ar^+ bombardment. In the first case the SEY decrease observed with the progressive conversion of sp^3 hybrids into six-fold aromatic domains was related to the electronic structure of the C-films close to the Fermi level. We found that a moderate structural quality of the C layer, corresponding to aromatic clusters of limited size, is sufficient to obtain a SEY as low as ~1. For the bombarded graphite, the strong lattice damage remains limited to the near surface layer, where the high density of defects reduces the transport of incoming and secondary electrons. Then, the SEY curves resulted differently modified in the low and high primary energy regions, but their maximal values remained favorably low. Our findings demonstrate that SEY, besides being an indispensable mean to qualify technical materials in many technological fields, can be also used as a flexible and advantageous diagnostics to probe surfaces and interfaces.

1. Introduction

Secondary Electron Yield (SEY) is an ubiquitous property of matter determining the actual behavior of a surface in a device and/or in a technologically relevant application. For instance, the use of low SEY surfaces is crucial for mitigating the multipacting effect, that is the uncontrolled multiplication of the secondary electrons emitted by technical materials hit by energetic electrons [1]. In accelerators, the prevision and the minimization of SEY are strict requirements to limit electron cloud phenomena and favor the stability of machine performances [2–5]. Analogous criticality concerns microwave and RF components for space applications, that find one of their most important functional limitations in the multipactor and corona breakdown discharges [6]. The urgency of these questions has led to diffuse investigations and now the importance of factors related to intrinsic material properties [7,8], morphology (roughness, structural disorder) [9,10], chemical state (reactivity, passivation, contamination) [11] and temperature (gas adsorption) [12,13] in determining the macroscopic SEY of materials hit by electron fluxes has been well assessed.

Usually, for a sample exposed to an electron beam the overall response of the material to external excitation is evaluated in terms of the standard quantities that characterize the SEY curve, namely its maximum δ_{max} and the corresponding primary electron energy E_{max} [5]. In this approach the very low energy (LE) part of the SEY curve is currently neglected. However, as it will be shown in the following, even if its contribution to the total SEY is not quantitatively relevant, it provides information on the ability of a surface to reflect primary electrons with kinetic energy close to zero. In some applications, such LE primary electrons are extremely significant and that their effect on SEY could effectively influence material performances. We show that LE-SEY is very sensitive to surface composition and its study provides direct and straightforward information on the chemical state of the surface and on the presence of minimal quantities of adsorbates. These aspects might become of primary importance for machine operating at low temperature.

In general, an efficient SEY reduction for materials exposed to high radiation doses could rely on the use of specific low emitting coatings, especially based on C, as it has been recently proposed for the base line design of parts of the high luminosity large hadron collider (HL-LHC) [14] and, potentially, for future circular colliders (FCC-hh) [4].The

* Corresponding author.
E-mail address: roberto.cimino@lnf.infn.it (R. Cimino).

https://doi.org/10.1016/j.elspec.2019.06.008
Received 17 July 2018; Received in revised form 3 April 2019; Accepted 20 June 2019
0368-2048/

beneficial effect of C coatings is usually related to the moderate SEY of the sp^2 hybridization, lower with respect to other hybridization states [15], as it has been ascertained for several nanographitic materials as fullerene [16], nanotubes [17], graphene [18,19] and graphene nanoplatelets [20]. The relevance of this issue makes the knowledge of the relation between microstructural and electronic properties of C materials and their macroscopic SEY highly desirable. On the other hand, C layers deposited on large areas, with techniques compatible with the geometry of accelerator components, may lack of high structural quality. Furthermore, even good graphitic layers, once exposed to electron, photon and ion fluxes during machine operation, might result severely damaged. It is therefore important to validate the SEY properties of graphitic films while their structural quality is altered by external factors.

In order to shed light on these points, in the last years we investigated the effect that the structural ordering of the C lattice has on the macroscopic SEY properties of ultrathin C layers. To this aim in a first study [8] we deposited amorphous C films on copper substrates and used X-ray (XPS) and ultraviolet (UPS) photoelectron spectroscopy, together with Raman spectroscopy, to follow *in situ* the $sp^3 \rightarrow sp^2$ structural reorganization and the coalescence of the sp^2 clusters into nanocrystalline graphite induced by thermal annealing, while probing in parallel the SEY properties of the samples. Moreover, in order to explore the opposite process, in a second study [9] we introduced controlled densities of crystal defects in a highly oriented pyrolytic graphite (HOPG) sample by subsequent cycles of Ar^+ ion bombardment at low kinetic energy (500 eV). Also in this case the effects of the lattice defects on the electronic, structural and secondary emission properties were monitored by measuring *in situ* UPS and XPS spectra together with SEY curves. Special attention was paid not only to the variation of the maximal SEY value, but also to more subtle changes on the entire curve, with a particular attention to the LE-SEY at low (< 40 eV) primary electron energy [21]. In the following we summarize the results and elucidate the discordant behavior observed for the two systems.

2. Experimental

The experiments were performed in the 'Material Science Laboratory' of the INFN-LNF at Frascati (Rome, Italy), in an ultra-high vacuum (UHV) system consisting of a preparation chamber and an analysis chamber, both having a base pressure of $2–5 \times 10^{-8}$ Pa. Polycrystalline Cu, Ag and Au substrates were cleaned by cycles of Ar^+ sputtering at 1.5 kV and prolonged thermal annealing at temperatures of ~1000 K. Carbon films were grown on polycrystalline Cu substrates at room temperature (RT) by radiofrequency magnetron sputtering using a power of 50 W and Ar pressure of 6 Pa. The thickness of the films used for this experiment was estimated to be of the order of 20 nm. Thermal annealing was performed in steps, by heating for 30 min the sample at a fixed temperature up to 1070 K. The temperature was measured by a calibrated pyrometer.

The HOPG sample was cleaved with adhesive tape before being loaded into the UHV system. Prolonged thermal annealing at temperatures of ~1000 K was carried out to desorb contaminants whose absence was crosschecked by XPS. The HOPG was Ar^+ ion bombarded at 500 eV and Ar pressure of 5×10^{-4} Pa for increasing doses up to $4.5 \times 10^{14} \pm 0.1\ Ar^+/cm^2$. After each ion dose, UPS and XPS analysis of the surface, as well as SEY measurements were carried out.

XPS and UPS measurements were performed by using an Omicron EA125 analyzer to reveal the photoelectrons excited by the non monochromatic radiation of Al Kα ($h\nu = 1486.7$ eV) or Mg Kα ($h\nu = 1254.6$ eV) and He II ($h\nu = 40.8$ eV) sources, respectively. The Raman spectra were measured using a Horiba XploRA Raman microscope system with a 100× objective at $\lambda = 532$ nm. Laser power was kept at 1 mW to avoid heat induced sample damage or graphitization. After the subtraction of the background due to the copper substrate the Raman spectra were best-fitted by using Gaussian and Lorentzian functions.

The SEY(δ) is defined as $SEY = \delta = I_{out}/I_p = (I_p\text{-}I_s)/I_p$, where I_p is the current of the primary electron beam hitting the sample, I_{out} is the current of the electrons emerging from the sample and I_s is the sample current to ground, as measured by a precision amperometer. SEY is measured as described in detail in Refs. [5,11]. In brief I_p (some tens of nA) was measured by means of a Faraday cup positively biased, whereas I_s was determined by biasing the sample at −75 V. SEY curves as a function of the primary energy E_p (referred to the Fermi level) are characterized by a maximum value (δ_{max}) reached in correspondence of a certain energy (E_{max}). As already discussed, [21] we can correctly measure SEY starting from few hundreds of meV above the sample work function. For all the experimental SEY data here shown, the measured curve drops from 1 to ~0 within an E_p region whose width (~0.85 eV) is determined by the thermally broadened electron beam emitted by a standard Ta disc cathode. SEY measurements are only valid after this drop, which occurs at an energy related to the surface vacuum level.

3. Results and discussion

3.1. Modification of the low-energy SEY of noble metals by surface adsorbates

For any material the yield of secondary electrons is influenced by the presence of a contaminating layer or even of submonolayer quantities of adsorbates [22]. Fig. 1 clearly summarizes how for noble metals the state of the surface affects their SEY curves. The grey curves in Fig. 1a–f shows the SEY and LE-SEY curves measured on "as received" polycrystalline Ag, Au and Cu samples. The curves exhibit the line shapes typical for metal surfaces examined before being cleaned in UHV, with the SEY rapidly rising up to E_p ~200 eV and decreasing for higher primary energies. δ_{max} values are 2.7, 2.0 and 2.1 for Ag, Au and Cu, respectively. In all cases the XPS spectra (Fig. 1g–i) shows intense O1s and C1s peaks determined by the presence of surface contamination due to the permanence of the samples in atmosphere.

Surface cleaning by Ar^+ (1.5 KeV) sputtering lowers the level of contamination below the XPS detection limit (red curves in Fig. 1g–i). Correspondingly, for all three metals, the SEY curves measured on the clean surfaces show values close to zero at very low E_p and remain well below 1.7 in the whole E_p range. In particular Cu shows the lowest δ_{max} (1.3), whereas moderately higher values are measured for Ag ($\delta_{max} = 1.65$) and Au ($\delta_{max} = 1.70$), in good agreement with previously published results [23,24].

As said, the transition from the regime where the incident electron beam is totally backscattered ($I_s = 0$, SEY = 1) to the regime where part of it is transmitted ($I_s \geq 0$, $SEY < 1$) corresponds to the vacuum level position. Therefore the energy separations measured among the vacuum levels of the three metals provide the differences between the corresponding work functions, being the Fermi level a common reference for the system. The data contain quantitative information on the surface work function: once we set the Cu work function to 4.6 eV the values derived for Au and Ag result 5.3 and 4.4 eV, respectively, in good agreement with the literature [25] In the 6-8 eV wide ranges above the transition region the SEY curves for all clean metals appear quite flat and reproduce the typical reflectivity curves measured for single crystal [26] and polycrystalline metals [27]. In fact, when E_p is only a few eV higher than the vacuum level, the efficiency of generating secondary electrons that escape from the solid is very low [28,29]. This implies that, for all the clean surfaces studied in this work, the reflection of very low energy electrons is extremely unfavorable, since they are mostly absorbed within the material. On the contrary, Fig. 1a, c and e show that all "as received" metals exhibit SEY higher than 0.5 for E_p above the transition region. Clearly, the presence of chemisorbed compounds, which modify the chemical bonds at the metal surface and, most importantly, interact directly with the impinging electrons, strongly affects the LE-SEY curves. Of course, the "as received" surfaces are not in

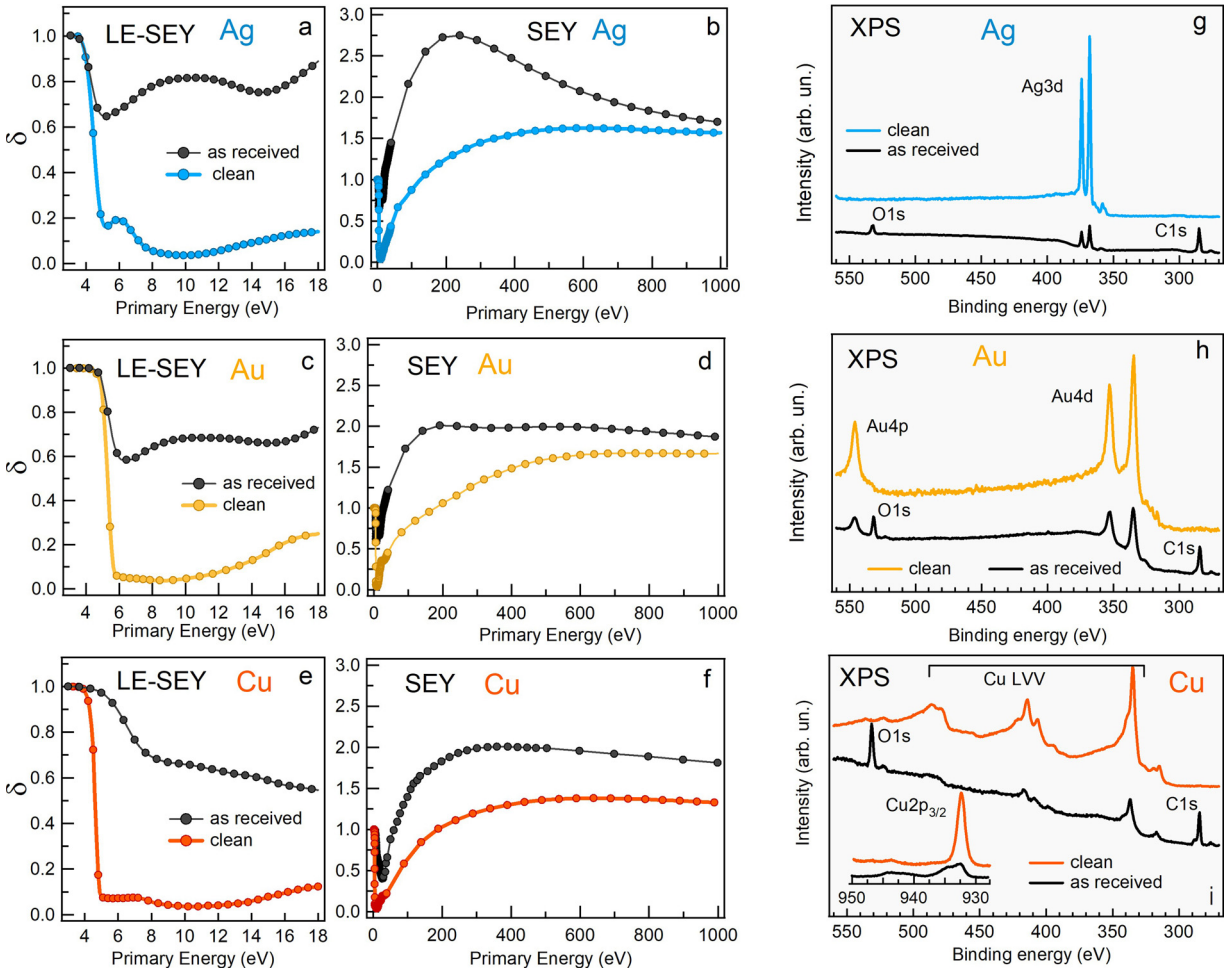

Fig. 1. (a, c, e) LE-SEY, (b, d, f) and SEY curves and (g, h, i) XPS spectra measured for clean and "as received" Ag, Au and Cu polycrystalline samples. In all cases the primary energy is referred to the Fermi Level. The inset in Fig.1i compares the high resolution spectra measured in the $Cu2p_{3/2}$ spectral region.

a well characterized chemical state and results can only be considered indicative of a trend. From a qualitative analysis, it turns out that Ag and Au both show a minimum in proximity of the transition region followed by a ~6 eV wide maximum and by a second minimum. This similarity suggests the presence of comparable contaminating layers that dominate the overall sample behavior. Differently, in the case of the "as received" Cu surface a continuous SEY decrease together with a net work function increase indicates a different chemical environment. In fact, in the XPS spectra measured on the "as received" metals (Fig. 1g–i) the O1s/C1s intensity ratio, that is less than 1 for Au and Ag, rises to 1.4 in the case of Cu, revealing the occurrence of metal oxidation. This is confirmed by the $Cu2p_{3/2}$ line shape showing a dominating oxide phase (see inset in Fig. 1i). Such a profound modification of the metal chemical state is not observed for the less reactive Au and Ag surfaces. The formation of an oxidized near surface layer in the Cu sample is likely responsible for the work function increase [30] observed in Fig. 1e.

The important effect that surface contaminants have on the secondary emission properties even in the absence of surface oxidation is well exemplified in Fig. 2a and b, which show the LE-SEY and SEY curves, respectively, measured at 10 K on the Cu sample clean and in the presence of controlled adsorbate layers [22]. The corresponding curves measured at RT on the clean Cu are also shown for comparison. The similarity between the curves measured on the clean metal at RT and at 10 K proves that cooling down the sample does not determine any strong SEY variation. However, keeping the sample at 10 K for some time determines the progressive adsorption of residual gas molecules (mainly H_2O, CO, CO_2 and CH_4, estimated total coverage ~0.3 ML) that modify mainly the LE-SEY curves. A stronger effect is observed when the clean metal is dosed with CO. In this case δ_{max} decreases with increasing coverage, becoming 1.3 and 1.2 after the adsorption of 0.5 and 1 ML of CO, respectively. An inverse behavior is observed in the LE-SEY region. The opposite trends in the low and high E_p regions can be reconciled by assuming that, at low E_p the presence of the adsorbed molecules reduces the number of impinging electrons penetrating the sample [31], due to enhanced surface scattering, and therefore increases the resulting δ value. On the other hand, the electrons impinging at high E_p massively penetrate the near surface layer, but the scattering due to the surface adsorbates damps the number of the secondary electrons emerging from the sample. The comparison between the curves taken with and without adsorbed CO indicates that a coverage of 1 ML is sufficient to deeply modify the LE-SEY curve proving the high surface sensitivity of this technique. Further studies in this direction could contribute to the understanding of the behavior of the inelastic mean free path for very slow electrons as discussed in recent experimental investigations [32,33].

3.2. The effect of the structural properties on the SEY of C materials

The relevance that thin C films have among low SEY materials is related to the optimal properties of graphitic carbon. These properties, however, tend to deteriorate when the C lattice becomes amorphous, that is when a certain percentage of C–C bonds loses the aromatic character and assume the tetragonal geometry of the sp^3 network. The

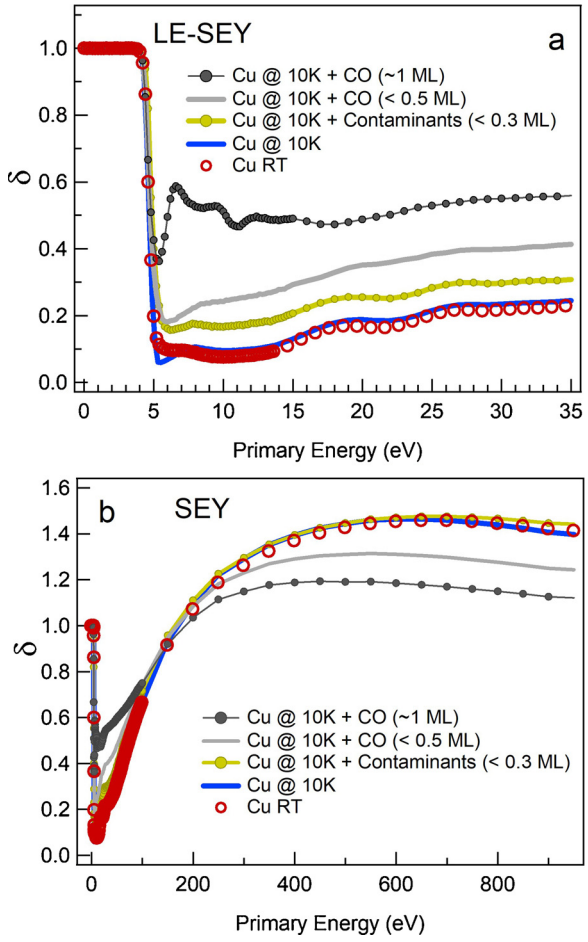

Fig. 2. (a) LE-SEY and (b) SEY curves measured at 10 K on a polycrystalline Cu sample clean (blue), covered by 0.3 ML of adsorbed residual gases (yellow) and covered by 0.5 ML (light grey) and 1 ML (dark grey) of CO. The LE-SEY and SEY curves measured on the clean sample at RT are shown for comparison (red\). In all cases the primary energy is referred to the Fermi level.

electronic and structural properties of the C lattice can be linked to its macroscopic secondary emission properties by inducing a controlled transition from a prevalent sp^3 to a prevalent sp^2 hybridization, and *vice versa*, while monitoring the evolution of the SEY curve [8]. To this aim we followed, in UHV, the thermal graphitization of ultrathin a–C layers and the amorphization of graphite HOPG by combining *in situ* the measurement of SEY curves with UPS and XPS spectroscopy. The investigation was then complemented by *ex-situ* Raman spectroscopy.

In Ref. [8] we deposited amorphous C films on copper substrates and followed *in situ* the $sp^3 \rightarrow sp^2$ structural reorganization and the coalescence of the sp^2 clusters into nanocrystalline graphite induced by thermal annealing [34–37], while acquiring at each step the SEY curve. Fig. 3a shows the survey XPS spectrum measured on the as-prepared a–C layer, whereas the evolution of the C1s, valence band and O1s spectra during thermal annealing is illustrated in Fig. 3b–e. The XPS spectrum in Fig. 1a shows the intense C1s peak at 284.5 eV and the weaker O1s peak at 532.5 eV. The latter is a typical feature observed in a–C films deposited by magnetron sputtering and is indicative of a 5–6% content of oxygen. The binding energy (BE) of C1s photoelectrons in C materials is related to the hybridization state of the emitting atoms and is a useful mean to estimate the sp^3/sp^2 ratio, since typically the sp^3 and sp^2 fingerprint components are found with a separation of 0.8–0.9 eV [35,38]. The upper curve in Fig. 3b shows the C1s spectrum measured on the as-deposited film which is peaked at 284.65 eV and exhibits a FWHM of 1.8 eV. The shift of 0.35 eV with respect to the position of the graphitic carbon (284.3 eV) indicates the presence a consistent fraction of sp^3 hybridized atoms. Accordingly, the valence band measured on the as-deposited layer (top curve in Fig. 3c) shows only a broad unstructured peak centered at 7.7 eV related to the σ bonds, consistent with the presence of sp^2 chains and limited aromatic domains coexisting with the sp^3 phase. In the Fermi level region the VB spectrum reveals the presence of an energy gap of ~0.4 eV (see Fig. 3d). With thermal annealing, the main σ peak progressively narrows and the feature related to the π band in graphite appears at ~3 eV indicating a rising concentration of the six-fold coordinated rings [35–37]. Fig. 3d shows that, in parallel, the density of states in the region close to the Fermi level increases and in the sample annealed at 1070 K resembles the quasi metallic character typical of the graphitic structures. Also the C1s peak manifests the occurrence of graphitization. It shifts to lower BE due to the progressive decrease of the sp^3 component, and after the annealing at 1070 K is peaked at 284.3 eV. Although this change indicates a substantial $sp^3 \rightarrow sp^2$ conversion, the wide spectral FWHM of the C1s peak (1.5 eV) reveals a low structural quality of the sp^2 network. Note that the C1s peak measured in the same experimental condition on HOPG exhibits a FWHM of 0.8 eV. Fig. 3e shows that with increasing annealing temperature the O1s intensity decreases while the peak down-shifts, likely indicating a modification of the chemical species forming the oxidized phase. The presence of a low percentage of oxidized C atoms, that photoemit between 285 and 288 eV [39], might contribute to the broadening of the C1s at the high BE side.

The evolution of the SEY and LE-SEY curves with thermal annealing is summarized in Fig. 3f and g. The slight δ_{max} decrease from 1.25 to 1.16 induced by the annealing to 710 K is followed by a more substantial reduction to 1.03 for the film annealed at 900 K, whereas after the last annealing step δ_{max} decreases to 0.99 and E_{max} shifts to 250 eV. The same trend indicating the SEY reduction is evident in the low energy region (Fig. 3g). By combining the information on the structural properties of the annealed film with the SEY curves, it comes out that the decrease in the SEY is directly related to the extent of graphitization.

Among the factors that might be at the origin of the observed behavior we can disregards the variation of the work function that for nanographitic C has been shown to decrease with graphitization [40], and would then correspond to an increase of SEY. Instead the behavior in the vicinity of the Fermi level can play a role. In a–C the presence of a gap at the Fermi level, setting a prohibited energy interval, reduces the probability for secondary electrons to lose energy through electron-electron collisions [16,41]. With the expansion of the graphitic domains induced by thermal annealing, the disappearance of the energy gap and the increasing number of electronic states close to the Fermi level likely rise the energy dissipation channels and reduce the diffusion length, thus effectively contributing to lower the yield of the secondary electrons emerging from the sample surface.

The level of microcrystalline disorder was quantified by considering the Raman spectra measured on the as-deposited and on the fully annealed layers (Fig. 3d) [8]. Spectral deconvolution shows the presence of broad D and G bands, together with two minor bands appearing at 1520 cm^{-1} (D3) and around 1200 cm^{-1} (D4). The G band arises from the vibrations of all sp^2 sites both in chain and ring configurations, whereas the D band originates only in clusters of sp^2 sites in six-fold aromatic rings [42]. D3 and D4 are both related to the presence of bond disorder in the material [43]. The main changes observed after thermal annealing at 1070 K are the higher D/G ratio and the narrower width of the G band, which also shifts from 1587 to 1603 cm^{-1}, confirming that the annealed material has reached the stage of nanocrystalline graphite [42].

Therefore during the graphitization a rise of the I(D)/I(G) ratio indicates the conversion of the carbon structures into aromatic rings, whereas at later stages, its decay is indicative of the expansion of the graphitic in-plane crystallite size L_α with the simultaneous drop of the edge defects concentration. It has been well established [42,44] that in

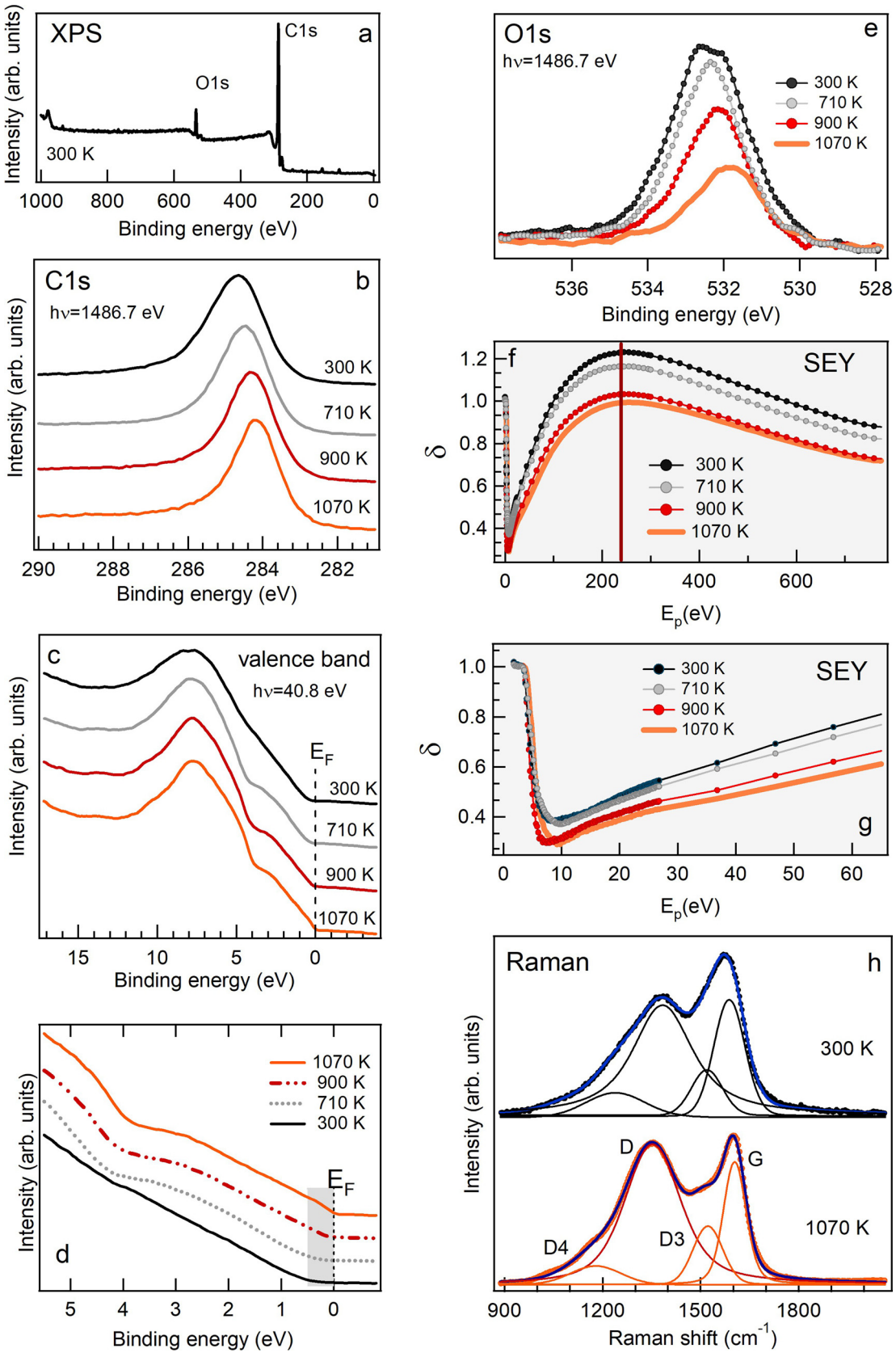

Fig. 3. (a) XPS spectrum measured on the as-prepared a–C layer. (b) C1s, (c) valence band spectra, (d) Fermi level region and (e) O1s spectra and (f) SEY and (g) LE-SEY curves measured on the C films as a function of the annealing temperature. (h) Raman spectra measured on the as-deposited C film (top) and after thermal annealing at 1070 K (bottom).

nanographitic materials with a large number of defects (typically in the transition stage from amorphous C to nanocrystalline graphite) the $I(D)/I(G)$ ratio and L_α are linked by the relation $I(D)/I(G) = C'(\lambda)L_\alpha^2$ with C′ (514 nm) ~0.55 nm^{-2}, whereas the Tuinstra and Koenig relation [45] $I(D)/I(G) = C(\lambda)/L_\alpha$, where C(514 nm) ~4.4 nm, is valid when the number of ordered rings rises and the crystallites reach dimensions of a few nanometers. The two relations used for pristine and annealed films, respectively, provide in turn L_α ~ 1.3 and 3.8 nm, confirming the moderate crystalline quality of the annealed film indicated by the width of the C1s peak.

It turns then out that the presence or aromatic clusters of a few nanometers in size is sufficient to lower the macroscopic SEY to the level of graphitic carbon with much higher structural ordering [8]. It is likely that in materials with small graphitic grains the enhanced scattering at the grain boundaries provides an additional contribution to reduce the number of secondary electrons emerging from the surface.

In Ref. [9] we started with a HOPG sample and introduced controlled amounts of defects in the crystalline lattice by subsequent cycles of Ar^+ ion bombardment at low kinetic energy (500 eV). Low energy ion bombardment can produce interstitial defects created by trapping incident ions underneath the carbon planes [46,47] and generate vacancies in the graphitic network. The structural defects are expected to change the electronic and structural properties of HOPG and consequently to affect its secondary emission properties. In Ref. [9] special attention was paid not only to the variation of δ_{max}, but also to the more subtle changes on the entire SEY curve, with a particular attention to the LE-SEY region.

The extent of Ar^+ induced HOPG amorphization was monitored by UPS spectroscopy of the valence band spectra measured at normal emission. Fig. 4a shows the spectrum of the intact HOPG exhibiting sharp features at 4.3 eV (σ band) and 7.5 eV (π band) [48]. The peak just above the Fermi Level is related to photoelectron emission excited by the He II satellite ($h\nu$ = 48.4 eV). Both σ and π bands decrease in intensity already at 1.2×10^{13} Ar^+/cm^2. The presence of broad unstructured features observed for doses higher than 5.0×10^{13} Ar^+/cm^2 indicates a total amorphization of the crystalline structure. The indications provided by the valence band spectra are paralleled by the evolution of the LE-SEY curves measured as a function of the ion dose (Fig. 4b). The curve measured on pristine HOPG shows features structures related to the elastic and inelastic electron-solid interactions, that provide direct information on the unoccupied band structure [49,50]. Such structured line shape is progressively smeared out as the ion dose increases, due to the loss of crystalline ordering after the nucleation of lattice defects. At dose of 1.5×10^{14} Ar^+/cm^2 the smooth curve profile is clearly indicative for the presence of strong disorder in the probed sample depth. As reporter previously [21], the absence of a significant reflected component for $E_p \leq 10$ eV in any LE-SEY curve shown in Fig. 4b is a signature of clean conducting surface, independent of the degree of crystallinity.

Complementary information is provided by the extended SEY curves shown in Fig. 4c. The intact HOPG exhibits a maximum value of 1.0 [3,16,51] for E_p in the 220-400 eV range. With rising ion dose, for in the high E_p region the SEY progressively decreases up to the ultimate value of 0.6. On the other hand in the low E_p region, δ_{max} rises to 1.1 for doses of the order of 15×10^{13} Ar^+/cm^2. We can then conclude that graphite maintains favorable secondary emission properties even when significantly defected. However the contrasting SEY behavior, that with increasing lattice defectivity rises at low E_p and decreases at high E_p, deserves a clarification.

It is interesting to compare this trend to the behavior observed in the previous paragraph during the graphitization of the a–C films. Whereas in that case thermal annealing determines a nearly constant SEY reduction for the whole E_p region, ion bombardment modifies selectively the SEY of HOPG. The discordant behavior is made more evident by plotting in Fig. 5a the δ_{max} values vs. annealing temperature measured for the first experiment, that show a trend consistent with the homogeneous graphitization of the whole layer, and in Fig. 5b the SEY values measured at E_p = 175 and 800 eV in the second experiment, showing at high E_p, but not at low E_p, the SEY drop with increasing sputtering dose.

Before going further it is important to point out that for the observed SEY evolution we can exclude any role due to modifications of the HOPG surface roughness [5], since atomic force microscopy showed only a minimal increase from 0.5 nm measured on the intact sample to 0.7 nm observed after the highest Ar^+ dose. Analogously, a possible role of a change in the work function can be also ruled out. Even if a

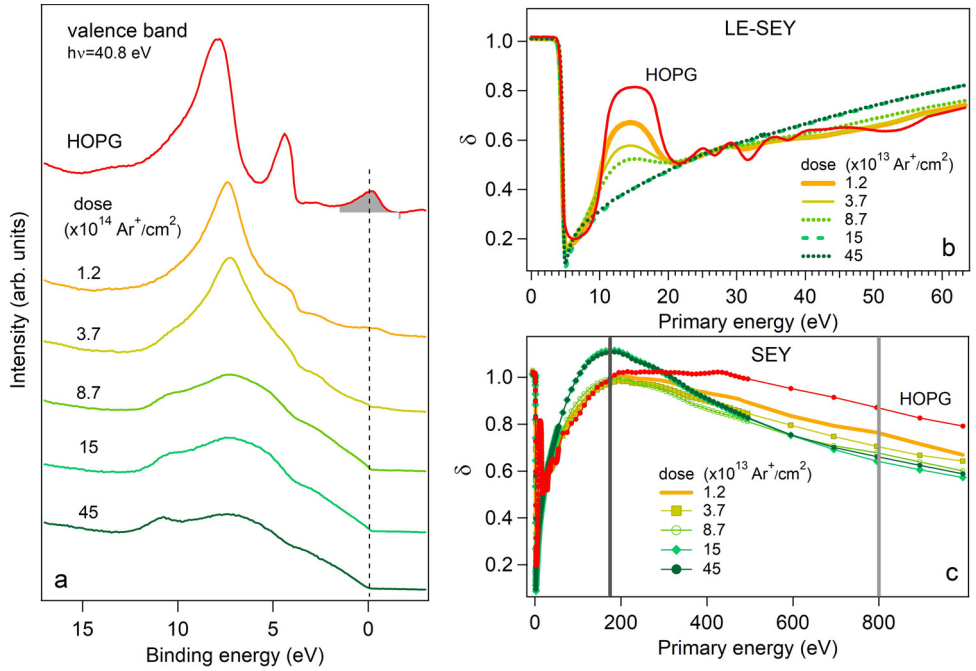

Fig. 4. (a) Valence band spectra (b) LE-SEY and (c) SEY curves measured on the pristine HOPG sample and after the exposure to increasing doses of Ar^+ ions with kinetic energy of 500 eV.

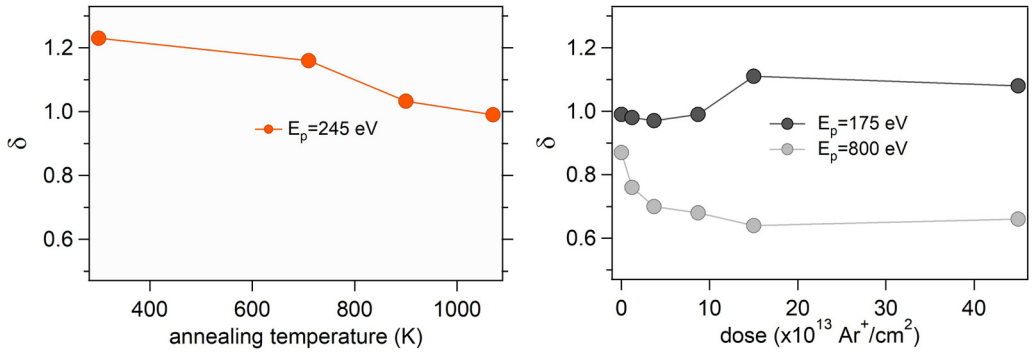

Fig. 5. *left*) δ_{max} values vs. annealing temperature measured during the graphitization of the a–C films (cfr. Fig. 3f) and *right*) δ values measured at E_p = 175 and 800 eV vs. the Ar^+ dose during the amorphization of HOPG (cfr. Fig 4 c).

work function increase of ~0.2 eV could be expected for graphite exposed to the Ar^+ ion doses used in this study [52], such a variation would have resulted in a SEY decrease in the whole E_p range, being higher the barrier that secondary electrons had to overcome to escape from the sample. In order to explain the observed results one must consider that the localized states that appear near the defect sites act as scattering centers for electron waves [53–56], which affect the transport properties of the damaged HOPG surface layer, decreasing the electron mean free path with respect to defect-free lattice. According to the estimation obtained by using the TRIM [57] software, the penetration depth of the 500 eV Ar ions impinging on HOPG is 1.9 ± 0.4 nm, in good agreement with previously published experimental data [58]. Then, ion bombardment produces a "bi-layered" structure, with the $l \sim 2$ nm thick damaged layer on top of the pristine HOPG bulk, and the transport properties of primary and secondary electrons depending on whether they move through the defected or through the intact graphitic lattice [9]. The primary electron penetration depth λ directly depends on the kinetic energy [59,60]. For 40 eV ≥ E_p ≥ 200 eV, the typical λ < 1 nm [61] decreases in the presence of defects, which means that primary electrons penetrate less than in the case of crystalline HOPG and that secondary electrons are produced in regions closer to the surface with a higher probability to escape to vacuum. On the other hand, defects damp the mean free path also for secondary electrons, limiting in principle their emergence from the sample. The SEY increase observed at E_p = 200 eV after very high Ar^+ doses is then the results of a fine play between different effects, likely including factors related to the shape and the size of the interaction volume and to the dependence of the scattering cross sections (at the defects) on the electron kinetic energy.

At E_p = 800 eV the kinetic energy of the primary electrons is sufficiently high that they will cross the damaged surface barrier. In that case the secondary electrons generated within the undamaged underlying HOPG, when traveling towards the surface with kinetic energies below 50 eV, suffer a significant mobility reduction [62] that hampers their escape into vacuum. This effect becomes more significant with increasing defect density at high ion doses. We believe that our data could trigger specific calculations and help to reach a more quantitative understanding of the effect of disorder and induced defects on transport and inelastic mean free path for carbon based materials.

4. Conclusions

In summary we have reported our recent results showing that the surface chemical state is a key factor in determining the SEY and LE-SEY properties of metal surfaces. Whereas clean metals exhibit SEY values that do not exceed 1.6 and are even lower in the case of copper, the presence of a contaminating layer can rise δ_{max} well above 2, while shifting the maximum of the SEY curves below 400 eV. More interestingly, the LE-SEY curves show heavy changes in the presence of adsorbates even at submonolayer coverage. Our results demonstrate that for very slow electrons the LE-SEY curve allows an easy measurement of the sample work function. For C materials our studies demonstrate that the SEY behavior and the structural properties are closely related. For amorphous C thin films the secondary emission decreases with the conversion of sp^3 hybrids to six-fold aromatic domains and the reason of that has been identified in the strong correlation between the electronic structure close to the Fermi level and the yield of secondary electrons. What is relevant is that a moderate structural quality of the C layer is sufficient for a considerable SEY decrease as aromatic clusters of limited size approach the secondary emission properties of graphite. This evidence might be exploited for the design and the optimization of ultrathin coating aimed at mitigating multipacting processes.

Amorphization of HOPG has been proved to modify the SEY curve, whose δ_{max}, however, remained stable and low (≤1.1) even in the presence of a high defect density. The LE-SEY results have shown that the absence of a significant reflected component, which is typical of clean conductors, is actually independent of the graphite crystalline quality. Moreover, the LE-SEY spectra resulted strongly dependent on the lattice ordering, which may have significant implications for simulations where SEY and LE-SEY curves are parametrized.

In conclusion we can remark that SEY and LE-SEY are valid tools, that, with a limited experimental requirement, can be used both to determine the response of materials to external excitation in terms of secondary electrons emission and as flexible and sensitive diagnostics to state surface cleanliness and to follow physical processes and chemical reactions occurring at surfaces.

Acknowledgements

This work was supported by the INFN (National Committee 5) Project MICA and by the Horizon 2020 Project "The European Circular Energy-Frontier Collider Study"(EuroCirCol) (grantNo654305). The authors wish to thank the DAFNE-L technical team for continuous assistance during the experiments.

References

[1] R.A. Kishek, Y.Y. Lau, Phys. Rev. Lett. 80 (1998) 193.
[2] M. Pivi, G. Collet, F. King, R.E. Kirby, T. Markiewicz, T. Raubenheimer, J. Seeman, F. LePimpec, Nucl. Instrum. Methods A 621 (1995) 47.
[3] R. Cimino, D. Grosso, M. Commisso, R. Flammini, R. Larciprete, Phys. Rev. Lett. 3 (2012) 2098.
[4] R. Cimino, V. Baglin, F. Schäfers, Phys. Rev. Lett. 115 (2015) 264804.
[5] R. Cimino, T. Demma, Int. J. Mod. Phys. A 29 (2014) 1430023.
[6] S.T. Lai, Fundamentals of Spacecraft Charging: Spacecraft Interactions with Space Plasmas, Princeton, NJ, 2002.
[7] C.Y. Vallgren, G. Arduini, J. Bauche, S. Calatroni, P. Chiggiato, K. Cornelis, P.C. Pinto, B. Henrist, E. Mètral, H. Neupert, G. Rumolo, E. Shaposhnikova, M. Taborelli, Phys. Rev. ST Accel. Beams 14 (2011) 071001.
[8] R. Larciprete, D. Grosso, A.D. Trolio, R. Cimino, Appl. Surf. Sci. 328 (2015) 356.

[9] L. Gonzalez, R. Larciprete, R. Cimino, AIP Adv. 6 (2016) 095117.
[10] R. Valizadeh, S. Malyshev, B.-T. Wang, Sian, Cropper, N. Sykes, Appl. Surf. Sci. 404 (2017) 370.
[11] R. Larciprete, D. Grosso, M. Commisso, R. Flammini, R. Cimino, Phys. Rev. ST Accel. Beams 16 (2013) 011002.
[12] J. Cazaux, Y. Bozhko, N. Hilleret, Phys. Rev. B 71 (2005) 035419.
[13] A. Kuzucan, H. Neupert, M. Taborelli, H. Störi, J. Vac. Sci. Technol. A 30 (2012) 051401.
[14] G. Apollinari, I. Béjar-Alonso, O. Brüning, P. Fessia, M. Lamont, L. Rossi, L. Tavian (Eds.), High Luminosity Large Hadron Collider (HL-LHC): Technical Design Report V. 0. 1, CERN Yellow Reports, Monographs, 2017, p. 4.
[15] M. Nishiwaki, S. Kato, J. Vac. Soc. Jpn. 118 (2005) 48.
[16] J.M. Ripalda, I. Montero, L. Vázquez, D. Raboso, L. Galán, J. Appl. Phys. 99 (2006) 043513.
[17] M.K. Alam, P. Yaghoobi, M. Chang, A. Nojeha, Appl. Phys. Lett. 97 (2010) 261902.
[18] J. Luo, P. Tian, C.-T. Pan, A.W. Robertson, J.H. Warner, E.W. Hill, G.A.D. Brigg, ACS Nano 5 (2011) 1047.
[19] H. Hiura, H. Miyazaki, K. Tsukagoshi, Appl. Phys. Exp. 3 (2010) 095101.
[20] I. Montero, L. Aguilera, M.E. Davila, V.C. Nistor, L.A. Gonzalez, L. Galan, D. Raboso, R. Ferritto, Appl. Surf. Sci. 291 (2014) 74.
[21] R. Cimino, L. Gonzalez, R. Larciprete, A. Di Gaspare, G. Iadarola, G. Rumolo, Phys. Rev. ST Accel. Beams 18 (2015) 051002.
[22] L.A. Gonzalez, M. Angelucci, R. Larciprete, R. Cimino, AIP Adv. 7 (2017) 115203.
[23] I. Bronshtein, B. Graiman, Secondary Electron Emission, Nauka, Moscow, 1969.
[24] H. Bruining, J.H. De Boer, Physica 5 (1938) 17.
[25] A. Kawano, Prog. Surf. Sci. 83 (2008) 1.
[26] P.L. Lévesque, H. Marchetto, T. Schmidt, F.C. Maier, H.-J. Freund, E. Umbach, J. Phys. Chem. C 120 (2016) 19271.
[27] N. Srivastava, Q. Gao, M. Widom, R.M. Feenstra, S. Nie, K.F. McCarty, I.V. Vlassiouk, Phys. Rev. B 87 (2013) 245414.
[28] R. Cimino, I. Collins, M.A. Furman, M. Pivi, F. Ruggiero, G. Rumolo, F. Zimmermann, Phys. Rev. Lett. 93 (2004) 014801.
[29] J. Cazaux, J. Appl. Phys. 111 (2012) 064903.
[30] J.A. Assimos, D. Trivich, Phys. Status Solidi (a) 26 (1974) 477.
[31] L.G. Caron, V. Cobut, G. Vachon, S. Robillard, Phys. Rev. B 41 (1990) 2693.
[32] D.P. Pappas, K.-P. Kämper, B.P. Miller, H. Hopster, D.E. Fowler, C.R. Brundle, A.C. Luntz, Z.-X. Shen, Phys. Rev. Lett. 66 (1991) 504.
[33] R. Zdyb, T.O. Menteş, A. Locatelli, M.A. Ni no, E. Bauer, Phys. Rev. B 87 (2013) 075436.
[34] R. Gago, M. Vinnichenko, H.U. Jäger, A.Y. Belov, I. Jiménez, N. Huang, H. Sun, M.F. Maitz, Phys. Rev. B 72 (2005) 014120.
[35] J. Diaz, G. Paolicelli, S. Ferrer, F. Comin, Phys. Rev. B 54 (1996) 8064.
[36] Y.V. Butenko, S. Krishnamurthy, A.K. Chakraborty, V.L. Kuznetsov, V.R. Dhanak, M.R.C. Hunt, L. Siller, Phys. Rev. B 71 (2005) 075420.
[37] R. Larciprete, S. Lizzit, S. Botti, C. Cepek, A. Goldoni, Phys. Rev. B 66 (2002) 121402.
[38] R. Haerle, E. Riedo, A. Pasquarello, A. Baldereschi, Phys. Rev. B 65 (2001) 045101.
[39] R. Larciprete, P. Lacovig, S. Gardonio, A. Baraldi, S. Lizzit, J. Phys. Chem C 116 (2012) 9900.
[40] A. Ilie, A.C. Ferrari, T. Yagi, S.E. Rodi, J. Robertson, E. Barborini, P. Milani, J. Appl. Phys. 90 (2001) 2024.
[41] N.E. Nickles, The Role of Bandgap in the Secondary Electron Emission of Small Bandgap Semiconductors: Studies of Graphitic Carbon. (All Graduate Theses and Dissertations. Paper 1696, (2002) http://digitalcommons.usu.edu/etd/1696.
[42] A. Ferrari, J. Robertson, Phys. Rev. B 61 (2000).
[43] A. Sadezky, H. Muckenhuber, H. Grothe, R. Niessner, U. Pöschl, Carbon 43 (2005) 1731.
[44] A.C. Ferrari, D.M. Basko, Nat. Nanothechnol. 8 (2013) 235.
[45] F. Tuinstra, J.L. Koenig, J. Phys. Chem. 53 (1970) 1126.
[46] J.R. Hahn, H. Kang, S. Song, I.C. Jeon, Phys. Rev. B 53 (1996) R1725.
[47] D. Marton, H. Bu, K.J. Boyd, S.S. Todorov, A.H. Al-Bayati, J.W. Rabalais, Surf. Sci. 326 (1995) L489.
[48] S.Y. Zhou, G.-H. Gweon, C.D. Spataru, J. Graf, D.-H. Lee, S.G. Louie, A. Lanzara, Phys. Rev. B 71 (2005) 161403.
[49] P.J. Mølert, M.H. Mohamed, J. Phys. C: Solid State Phys. 15 (1982) 6457.
[50] R.F. Willis, B. Fitton, G.S. Painter, Phys. Rev. B 9 (1974) 1926.
[51] N.R. Whetten, J. Appl. Phys. 34 (1963) 771.
[52] H. Hashimoto, M. Watanabe, S. Nishiuma, K. Nakamura, S. Yoshida, Surf. Interfaces Anal. 35 (2016) 19.
[53] T. Tanabe, Phys. Scr. 1996 (1996) 7.
[54] N. Gorjizadeh, A.A. Farajian, Y. Kawazoe, Nanotechnology 20 (2009) 015201.
[55] D.L. Maslov, V.I. Yudson, A.M. Somoza, M. Ortuño, Phys. Rev. Lett. 102 (2009) 216601.
[56] F. Banhart, J. Kotakoski, A.V. Krasheninnikov, ACS Nano 5 (2010) 26.
[57] J.F. Ziegler, M.D. Ziegler, J.P. Biersack, Nucl. Instrum. Methods B 268 (2010) 1818.
[58] T. Li, B.V. King, R.J. MacDonald, G.F. Cotterill, D.J. O'Connor, Q. Yang, Surf. Sci. 312 (1994) 399.
[59] G.F. Dionne, J. Appl. Phys. 44 (1973) 5361.
[60] G.F. Dionne, J. Appl. Phys. 46 (1978) 3347.
[61] M.P. Seah, W.A. Dench, Surf. Interfaces Anal. 1 (1979) 1.
[62] A. Lherbier, B. Biel, Y.-M. Niquet, S. Roche, Phys. Rev. Lett. 100 (2008) 036803.